Water vapour and cloud observations by lidar during a front passage

P.Di Girolamo[a], P.F. Ambrico[b], A. Amodeo[b], A. Boselli[b], M. Pandolfi[b], G. Pappalardo[b], N. Spinelli[c], V. Cuomo[a,b]

[a] *Dipartimento di Ingegneria e Fisica dell'Ambiente, Università della Basilicata, viale della Tecnica 3, Potenza I-85100, ITALY*
[b] *Istituto di Metodologie Avanzate di Analisi Ambientale, C.N.R., C.da S.Loja, Tito Scalo I-85050, ITALY*
[c] *Dipartimento di Scienze Fisiche, Università "Federico II", via Cintia, Napoli I-80136, ITALY*

ABSTRACT

Atmospheric water vapour plays a crucial role in the microphysical processes leading to cloud formation and development. The role of atmospheric water vapour in cloud formation processes can be accurately determined by means of remote sensing techniques.

Lidar techniques can accomplish ground-based measurements of atmospheric water vapour and cloud properties with high space and time resolution. A lidar system capable to perform simultaneous measurements of atmospheric water vapour and clouds has been developed in Potenza, Southern Italy.

Several lidar measurement campaigns were performed in Potenza. The campaigns were primarily aimed to the measurements of tropospheric aerosol and water vapour content. Lidar aerosol measurements have been performed both in the UV and VIS spectral ranges, while water vapour measurements have been accomplished by using both the Raman (UV) and D.I.A.L. (near IR) techniques; these measurements have been compared with simultaneous radiosonde data obtained from both free and captive balloons.

Lidar measurements allowed obtaining information on cloud physical and optical properties. Water vapour and cloud properties measurements performed both in fair weather conditions and during a front passage are reported and discussed.

1 INTRODUCTION

Atmospheric water vapour and clouds play a crucial role in the Earth climate system, being key elements in the global radiation budget.

The role of atmospheric water vapour and clouds in the climate system results to be only partially comprehended at present, as a result of their highly variable time and space distribution on the global scale.

Clouds are particularly important in the atmospheric radiation budget. In fact the amount of solar radiation reaching the Earth surface is strongly dependent on the cloud coverage and on the microphysical properties of the clouds. Their presence, type, and height can also play an important role in the balance of the upwelling infrared radiation. As a consequence cloud can influence not only the Earth temperature, but also the local meteorology and the global climate.

Due to their high spatial and temporal variability, cloud parameters are difficult to measure and to model. At the present clouds are one of the most important parameters to include in any accurate global climate model.

High temporal and spatial resolution measurements by both space-borne and ground-based instruments are therefore necessary to monitor atmospheric water vapour and clouds for climate purposes. Lidar techniques can accomplish ground-based measurements of atmospheric water vapour and clouds with high space and time resolution. A Raman lidar can accomplish water vapour measurements especially in night time conditions. Water vapour measurements through the Raman technique are based on the simultaneous detection of the backscattered radiation in the vibrational Raman bands of water vapour and molecular nitrogen. In order to calibrate the system Raman measurements have been compared with radiosonde data obtained from both free and captive balloons launched in Potenza simultaneously or almost simultaneously to lidar operation.

Measurements of cloud physical properties such as cloud base height; cloud vertical extent can also be accomplished by lidar. Moreover lidar can provide information on the volume backscattering, extinction coefficient, and optical depth of the cloud, as well as depolarisation ratio, which can be interpreted in terms of the physical properties of cloud particles.

In the present paper we discuss the methodology used in order to retrieve the physical and optical properties of clouds.

2 EXPERIMENTAL APPARATUS

The Potenza lidar system has been developed around a Nd:YAG laser source operating on both second and third harmonics (532 and 355 nm). The main characteristics of the system are reported in table 1.

TABLE 1: Characteristics of the lidar system in the UV-VIS spectral region

LASER SOURCES	
Nd:YAG laser	
Wavelength and pulse energy	*λ=1064nm E=600mJ* *λ=532nm E=300mJ* *λ=355nm E=170mJ*
Pulse duration	*10 ns*
Pulse repetition rate	*20 Hz*
Beam divergence	*<0.5 mrad*
Dye laser	
Tunable range	*690-730 nm (Rhodamine 700)*
Linewidth	*0.12 cm^{-1}*
Divergence	*≤0.5 mrad*
Pulsewidth	*< pump laser*
Equipped with a dual wavelength device	
RECEIVER	
Telescope in Cassegrain configuration	
Diameter primary mirror	*0.5m*
Combined focal length	*5m*
Field of view	*0.2 - 1 mrad*
SPECTRAL SELECTION	
Double-grating monochromator *(used in the Raman channels)*	
Bandwidth	*2.0 nm*
Grating efficiency	*30%*
Out of band rejection	*10^{-8}*
Filters	
Bandwidth	*<2 nm*
Peak transmission	*>60%*
Out of band rejection	*$<10^{-6}$*
Single-grating monochromator *(used in the DIAL channel)*	
Bandwidth	*4.0 nm*
Grating efficiency	*30%*
Out of band rejection	*10^{-6}*
DETECTORS	
Photomultipliers (enclosed in cooled housing)	

The 355 nm laser beam, used to stimulate Raman scattering by water vapour and nitrogen molecules (407.5 and 386.6 nm, respectively), allows to perform humidity lidar measurements through the application of the Raman technique.

Backscattering and extinction coefficient measurements are performed both at 355 nm and 532 nm.

The receiver was developed around a vertically pointing Cassegrain telescope (0.5 m diameter primary mirror). Double grating monochromators and interference filters are used as spectral selection devices, while the selected radiation is detected by means of cooled photomultipliers, whose output signals are amplified and sampled by means of both photon counting and analog-to-digital conversion. Measurements vertical resolution ranges from 3 to 300 m.

A detailed description of the system is reported in a previous paper (Ambrico et al., 1997)

3 LIDAR THEORY

The basic Lidar principle is the following: a laser pulse is transmitted into the atmosphere where it encounters gas molecules and particles; a small amount of this energy is backscattered in the direction of the receiver system, typically a telescope, and transferred to a photodetector as a photo-multiplier. The resulting electrical signal is proportional to the optical power received, which depends on the presence, range and concentration of atmospheric scatterers and absorbers. In the monostatic configuration both transmitter and receiver are located in the same place. In this case, with the assumption of single scattering, the received optical power, $P(\lambda, \lambda_L, z)$, at wavelength λ, as a function of range z and the laser wavelength λ_L, is given by the expression (Measures, 1984):

$$P(\lambda,\lambda_L,z) = P_0 \frac{A \cdot O(z)}{z^2}\left(\frac{c\tau}{2}\right)\eta\beta(\lambda,\lambda_L,z)\exp\left\{-\int_0^z [\alpha(\lambda,z') + \alpha(\lambda_L,z')]dz'\right\} \quad (1)$$

where P_0 is the transmitted power, A the receiver aperture area, O(z) the overlap function between the laser beam and the field of view of the receiver, c the light velocity, τ the laser pulse duration, η the detection efficiency and $\beta(\lambda,\lambda_L,z)$ and $\alpha(\lambda,z)$ the backscattering and extinction coefficients of the atmosphere as a function of wavelength. $\beta(\lambda,\lambda_L,z)$, as well as $\alpha(\lambda,z)$, is the sum of contributions from both molecules ($\beta_m(\lambda, \lambda_L,z)$, $\alpha_m(\lambda,z)$) and aerosols ($\beta_A(\lambda, \lambda_L,z)$, $\alpha_A(\lambda,z)$):

$$\beta(\lambda,\lambda_L z) = \sigma_\beta(\lambda,\lambda_L)\rho_m(z) + \beta_A(\lambda,\lambda_L z), \quad (2a)$$

$$\alpha(\lambda,z) = \sigma_\alpha(\lambda)\rho_m(z) + \alpha_A(\lambda,z), \quad (2b)$$

where $\sigma_\beta(\lambda,\lambda_L)$ and $\sigma_\alpha(\lambda)$ are the molecular backscattering and extinction cross-sections, $\beta_A(\lambda, \lambda_L,z)$ and $\alpha_A(\lambda,z)$ are the aerosol backscattering and extinction coefficients, and $\rho_m(z)$ is the molecular density profile.

If received and transmitted wavelengths are coincident, as in the case of elastic scattering, eqn. 1 can be written as:

$$P(\lambda, z) = P_0 \frac{A \cdot O(z)}{z^2}\left(\frac{c\tau}{2}\right)\eta\beta(\lambda, z)\exp\left[-2\int_0^z \alpha(\lambda, z')dz'\right] . \qquad (3)$$

A Raman technique measurement of water vapour is accomplished by the simultaneous detection of the backscattered radiation from the vibrational Raman bands of water vapour and molecular nitrogen. The ratio between the water vapour number density $n_{H_2O}(z)$ and the ambient gas number density n(z) ($x_{H_2O}(z)=n_{H_2O}(z)/n(z)$), known as water vapour mixing ratio $x_{H_2O}(z)$, is evaluated through the following expression:

$$x_{H_2O}(z) = 0.78 \frac{P_{H_2O}(z)}{P_{N_2}(z)} \frac{k'}{k''} \frac{\sigma_{N_2}}{\sigma_{H_2O}} \frac{T_{\lambda_{N_2}}(z)}{T_{\lambda_{H_2O}}(z)} \qquad (4)$$

with $P_{H_20}(z)$ and $P_{N_2}(z)$ being respectively the Raman backscattered radiation by water vapour and nitrogen molecules, σ_{H_2O} and σ_{N_2} being the Raman cross sections for the two species, $n_{H_2O}(z)$ and $n_{N_2}(z)$ being their number densities, and $T_{\lambda_{N2}}(z)$ and $T_{\lambda_{H20}}(z)$ being the transmissivity of the atmosphere at λ_{N_2} and λ_{H_2O}, respectively. k' and k" are the optical efficiencies of the Raman channel at λ_{N_2} and λ_{H_2O}, respectively, and are dependent on the transmission and detection efficiencies at the two wavelengths. The ratio method makes atmospheric water vapour measurements simply determinable from lidar signals, the major limitation being represented by the small Raman scattering cross section (10^{-30} cm^2 sr^{-1} against 10^{-27} cm^2 sr^{-1} for Rayleigh scattering) and consequently the limited vertical range monitored (never exceeding 10-12 km).

In the following analysis we do not take into account the multiple scattering contribution to the backscattered signal. The small angular aperture of the telescope (i.e. small field of view) and of the laser beam justifies this assumption.

4 WATER VAPOUR MEASUREMENTS

Water vapour measurements by the Raman techniques have been performed on different nights during the period Jan.-Feb. 1997. Figure 1 reports intercomparisons between Raman water vapour profiles and simultaneous radiosonde. If radiosonde data are used as reference measurements, the comparison between the two techniques allows to estimate the calibration coefficient for Raman measurements.

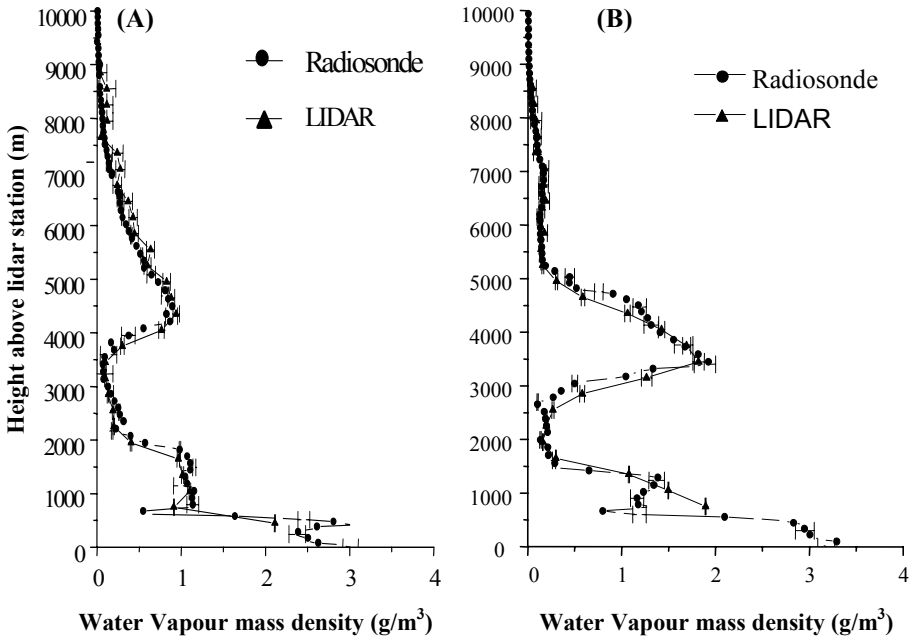

Fig. 1. Water vapour profile from lidar and radiosonde data measured in Potenza at: a) 19:15-19:45 GMT- on 18 February 1997; b) 22:45-23:15 GMT- on 18 February 1997

The water vapour Raman profiles are characterised by a vertical resolution of 300 m up to an altitude of approximately 9 km; the water vapour content is expressed in terms of water vapour mass density (g/m^3). Both Raman profiles

are obtained by integrating lidar measurements over 30 minutes: from 19:15 to 19:45 GMT (fig. 1A) and from 22:45 to 23:15 GMT (fig. 1B). Radiosondes have been launched at 19:35 GMT and 22:55 GMT respectively. Data integration over 30 minutes is performed in order to reduce the statistical error affecting Raman measurements (better than 10 % up to 6 km of height). The accordance between Raman and radiosonde water vapour profiles is good for both cases (10 % up to 5 km of height), except for the values within the lower 700 m a.g.l. The disagreement between two techniques below this level is due to the fact that the Raman technique was optimised to measure water vapour concentrations up to 9 km. Consequently the telescope and laser beam fields of view overlap only above about 700 m of height.

In order to limit the effect of this problem atmospheric water vapour content measurements have been performed through the simultaneous application of the Raman and DIAL techniques, with dial measurements optimised for the Planetary Boundary Layer.

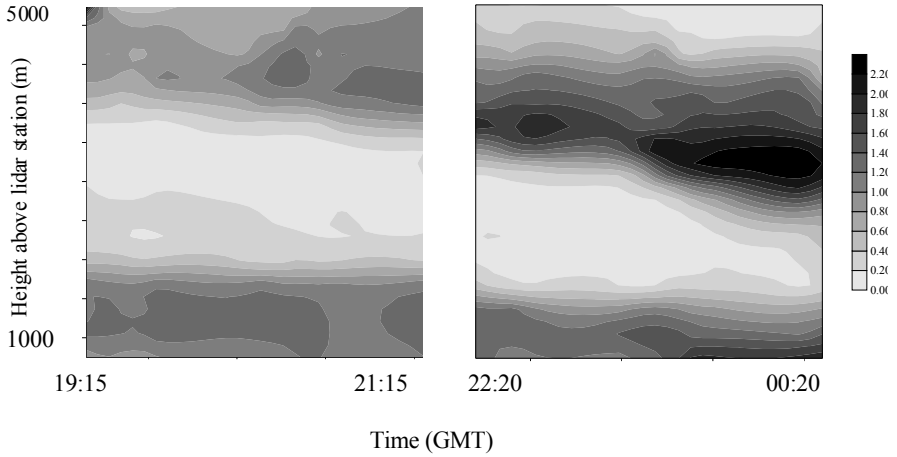

Fig. 2. Contour map representing the time evolution of the atmospheric water vapour mass density (g/m^3) in Potenza on 18 February 1997.

The map in fig. 2 represents the time evolution of the atmospheric humidity distribution, extending up to 5 km above the lidar station, during 4 hours of measurement (from 19:15 to 21:15 and from 22:20 to 00:20 GMT, on 18 February 1997), as determined by the Raman technique. The measurement was started after sunset, two humidity layers are present within troposphere: a lower layer extending up to approximately 3.5 km and an upper level up to approximately 9 Km. METEOSAT satellite images clearly show the presence of a warm frontal zone passing during the night of the 18th February, over the lidar station in Potenza. The warmer and more humid air passing over the station is

evident in the map. Moreover radiosonde launches confirm that warmer advecting air is incoming and taking the place of colder air stationing above the station in the evening. Moreover in the lower atmosphere the reduction of the sun driven convective activity is also evident. As an indication of this phenomenon at 19:15 GMT, that is almost three hours after sunset, the humidity layer present in the first 2 km tend to descend to lower levels where values are increasing with time.

5 CLOUD PROPERTIES

5.1 CLOUD PHYSICAL PROPERTIES

Cloud physical properties can be determined from elastic lidar signal on the basis of quite simple considerations (S.R. Pal et al., 1992). In principle the lidar signal in a homogeneous atmosphere is an exponential decreasing function (eqn.3). If a cloud is present, the lidar signal increases as a result of a larger amount of the backscattered radiation. Figure 3.B represent an elastic signal at 532 nm, taken in Potenza on August 11th, 1999 at 7:23 GMT. Two clouds are present in the altitude range 4 - 5 Km.

Cloud base height (r_b), cloud top (r_t) and cloud peak (r_p) can be evaluated from the derivative of the lidar signal.

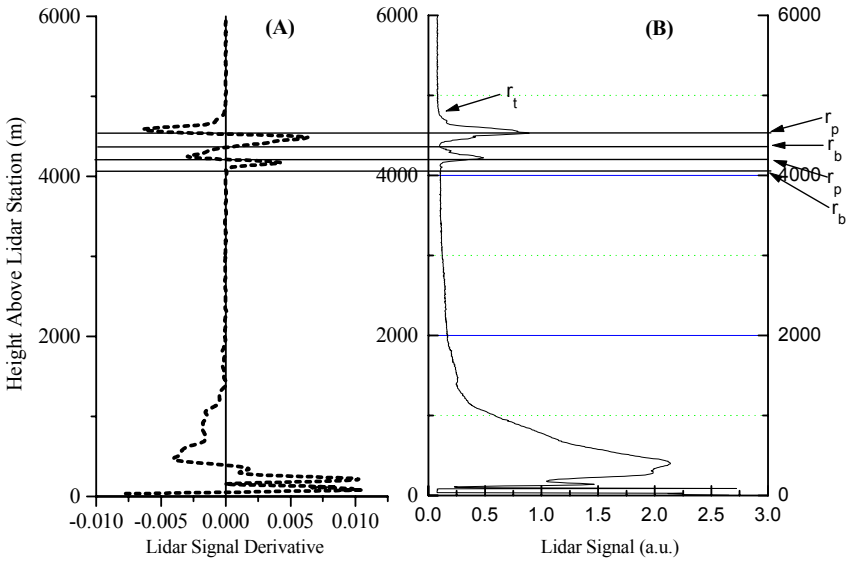

Fig. 3 Evaluation of the cloud base, peak and top from a lidar return and its derivative

Cloud base and cloud peak heights can be determined by considering the zero crossing derivative. For the cloud base the derivative gets values from negative to positive while for cloud peak the derivative gets values from positive to negative. We must point out that in the case of measured signals particular care must be taken of the spurious zero crossing due to aerosol load and inhomogeneities. Moreover other zero crossing level not related to the cloud presence can be due to noise.

In order to reject these spurious zero crossing when evaluating the derivative also the signal (if it is possible a signal without cloud) must be used to distinguish them from the cloud case.

For the cloud top there are two possible cases. If the cloud is thin, i.e. there is a non zero signal after the cloud, the cloud top height can be considered as the height where the lidar signal becomes smaller or equal to the expected signal above the cloud. If the cloud is thick, the cloud top height can be only evaluated as the level above the cloud where the signal becomes zero.

In figure 4 the cloud base height evolution with time has been reported for 45 minutes of measurements on the 10 June 1999 with a temporal resolution of 3 minutes.

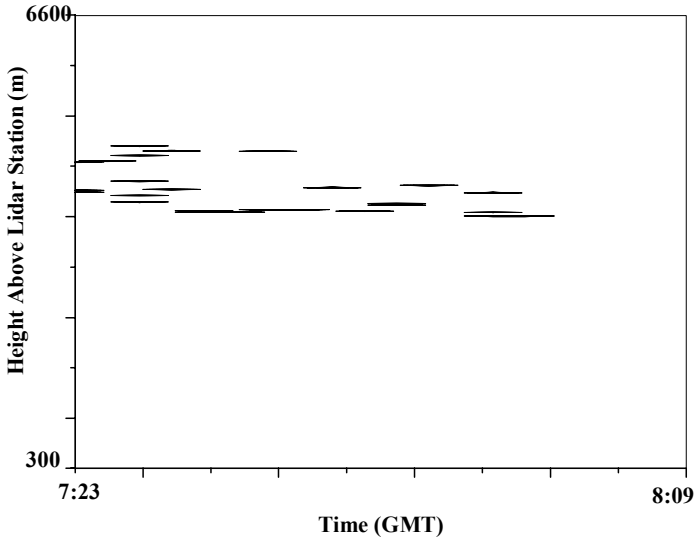

Fig.4 Time Evolution of the cloud base, Potenza June 10, 1999.

5.2 CLOUD OPTICAL PROPERTIES

Cloud optical properties such as optical depth, backscattering, and extinction can be accurately measured by the lidar technique. Figure 5 shows the temporal

evolution of the transmissivity (Cuomo et al., 1995) profile during a night of measurement (September 18, 1998) as obtained from the molecular nitrogen Raman return signal at 386.6 nm. Three different transmissivity profiles, each one based on an integration time of 30 minutes (36000 laser shots), are shown. The first measurement started at 18:28 GMT, just two hours after sunset; this profile shows a marked extinction between 8.5 Km and 10.5 Km, due to the presence of a cirrus cloud. In the second measurement, started at 23:10 GMT no clear evidence of cloud extinction is present, as it is also shown by the last data set acquired after 02:22 GMT.

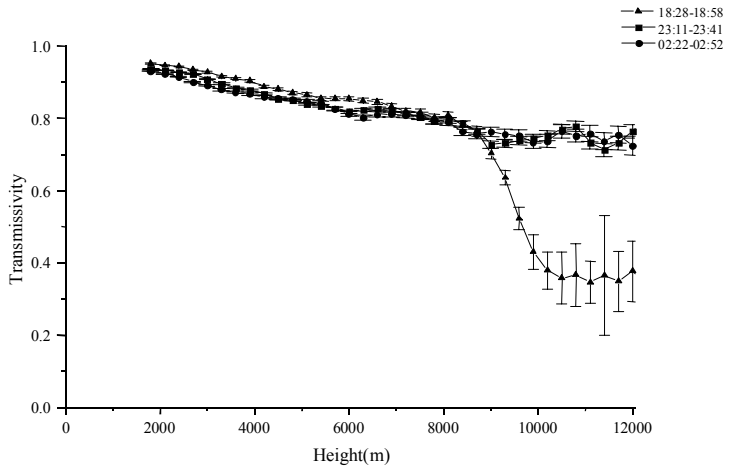

Fig.5: Atmospheric transmissivity profiles obtained in Potenza on September 18, 1998.

The aerosol backscattering coefficient β_A during the cloud passage (18:28-18:58 GMT) was determined from the lidar elastic signal at λ=355nm by using the procedure defined by Di Girolamo et al. (1996, 1999).

The aerosol extinction profile is also obtained from the lidar return signal at the molecular nitrogen Raman shifted wavelength through the Ansmann et al. (1992) algorithm. Measurements of the aerosol backscattering and extinction coefficients are simultaneous and independent.

Figure 6 illustrates the aerosol backscattering and extinction coefficient during the cirrus cloud passage. In this figure the presence of the cloud extending from 8.5 km up to 10.5 km is evident. The optical thickness of the cloud is 0.7±0.1, while the peak aerosol backscattering is $6{,}5 \times 10^{-5} cm^{-1} sr^{-1}$ at 9.3 km. Once again the integration time is 30 minutes; during this time interval the cloud optical and physical properties display a very limited variability with time and height. From the simultaneous and independent measurements of the extinction and backscattering coefficients the cloud lidar ratio K_{355} is obtained.

Within the cloud K_{355} is variable between 8 and 21 sr such values being typical of a cirrus cloud, as reported in literature (Ansmann et al., 1992).

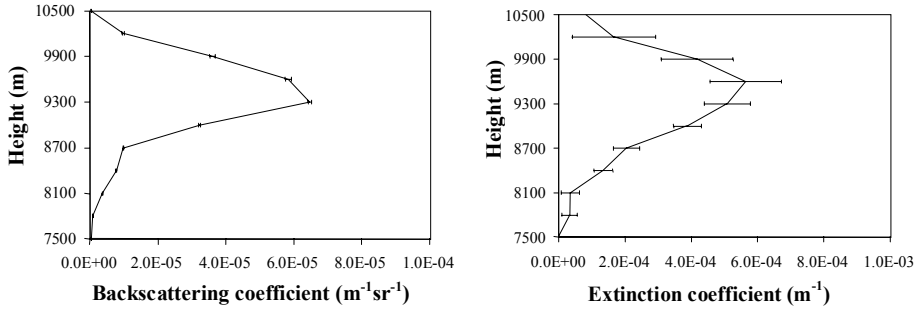

Fig.6 Cloud backscattering and extinction coefficient, Potenza September 18, 1998.

The lidar ratio profile reported in fig.7 shows smaller values of the lidar ratio in the region of stronger backscattering, numerical calculations indicate the lidar ratio to decrease with the decreasing of particles size in the cloud; smaller particles associated with larger backscattering values may indicate a larger concentration of smaller particles in the central region of the cloud, with collision and coalescence mechanisms producing an increase of their sizes together with a decreasing of their concentration.

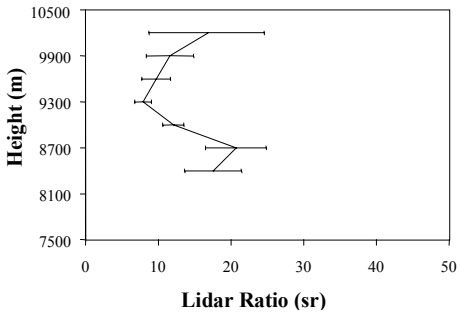

Fig. 7 Cloud lidar ratio, Potenza September 18, 1998.

6 CONCLUSION

In the present paper we demonstrated how a lidar system can be used in order to monitor the spatial distribution of atmospheric parameters and their evolution with time. We illustrated results evidencing that the lidar technique is a particularly reliable tool to accomplish ground-based measurements of

atmospheric water vapour and clouds with high space and time resolution. A Raman lidar has been used in order to perform water vapour measurements at night time. Raman measurements have been compared with radiosonde data obtained from both free and captive balloons launched in Potenza simultaneously or almost simultaneously to lidar operation. The agreement between sonde and lidar is within 10%. The time evolution of the water vapour mixing ratio has been studied during a selected night of measurements. The lidar measurements supported by radiosonde launches suggest the presence of a frontal zone passing over the station. Satellite images confirmed this observation.

Measurements of cloud physical properties such as cloud base height, cloud vertical extent have been shown together with backscattering and extinction coefficients. The measured lidar ratio for the reported case enables us to classified the observed cloud as a cirrus.

6 REFERENCE

Ambrico P.F., Amodeo A., Amoruso S., Armenante M., Berardi V., Boselli A., Bruzzese R., Capobianco R., Di Girolamo P., Fiorani L., Pappalardo G., Spinelli N., Velotta R., A multiparametric LIDAR system spanning from UV to the mid IR*, Laser und Optoelektronic,* 1997, **29**, 62-69.

Ansmann A., Wandiger U., Riebesell M., Wietkamp C., Michaelis W., Indipendent measurement of exctinction adn backscattere profiles in cirrus clouds by using a combined Raman elastic-backscatter lidar, *Applied Optics*, 1992, **31**, 7113-7131.

Cuomo V., Di Girolamo P., Gagliardi R.V., Pappalardo G., Spinelli N., Velotta R., Boselli A., Berardi V., Bartoli B., Lidar measurements of atmospheric transmissivity*, Il Nuovo Cimento* 1995, **18**, 209-222.

Di Girolamo P., Pappalardo G., Spinelli N., Berardi V., Velotta R., Lidar observation of the stratospheric aerosol layer over southern Italy in the period 1991-1995, *Journal of Geophisi. Research*, 1996, **101**, 18,765-18,773.

Di Girolamo P., Ambrico P.F., Amodeo A., Boselli A., Pappalardo G., Spinelli N., "Aerosol Observations by lidar in the nocturnal boundary layer", *Applied Optics*, 1999, **38**, 4585-4595.

Measures R. M., Laser Remote Sensing: Fundamentals and Applications, Wiley, New York (1984).

Pal S.R., Steinbrecht W., Carswell A.I., Automated method for lidar determination of cloud-base height and vertical extent, Applied Optics, 1992, **31**, 1488-1494.